Can we detect convection in the Sun?

Shravan M. Hanasoge[1], T. L. Duvall, Jr.[2], M. L. Derosa[3] and M. S. Miesch[4]

[1]W. W. Hansen Experimental Laboratory, Stanford University, Stanford, CA 94305, USA
email: shravan@stanford.edu
[2]Laboratory for Solar and Space Physics, NASA/Goddard Space Flight Center, Greenbelt, MD 20771,USA
[3]Lockheed Martin Solar and Astrophysics Laboratory, Palo Alto, CA 94304, USA
[4]HAO, NCAR, Boulder, CO 80307, USA

Abstract. We investigate the possibility of detecting deep convection in the Sun by computing travel-time shifts induced by convective flows interacting with propagating waves. The convection zone is modeled using a velocity profile taken from an Anelastic convection simulation. We present results obtained from a ray calculation of travel-time shifts. We compare these results with a full 3D calculation of the wave-flow interaction.

Keywords. Waves, convection, Sun: helioseismology, Sun: oscillations

1. Introduction

Many investigators have attempted to detect deep convection (e.g. Zhao & Kosovichev 2004), with some efforts focused on isolating giant cell signatures (e.g. Beck, Duvall, & Scherrer 1998) from solar data. Despite these efforts, giant cells have not been observed, perhaps due to the relatively small surface velocities they are estimated to possess (e.g. van Ballegooijen 1986). Furthermore, there have been no convincing observations relating to sub-surface convective activity below the supergranular layer. Swisdak & Zweibel (1999) have shown that solar eigenfrequency shifts may also be poor diagnostic agents because of their weak sensitivity to large scale convection, the effects of which appear only at the second order.

We show in this paper that time-distance helioseismology (Duvall *et al.* 1993) applied to extract signatures of deep convection may prove to be a promising technique. Time-distance helioseismology is based on measuring wave travel times from one surface location to another to investigate properties along the wave propagation pathways between these locations. In rough summary, signals at these two regions are cross-correlated and analyzed to recover the wave travel times. There are two principal diagnostic agents, the mean travel-time and the travel-time difference, the former being predominantly sensitive to sound speed perturbations and the latter to flows.

It is known that very small thermal perturbations are sufficient to sustain deep convective activity. Convective velocities in the interior, estimated from simulations and otherwise, are placed at 100 ms^{-1}, which in terms of travel-time shifts is arguably a stronger effect than sound speed flucatuations, a direct effect of the convection induced thermal fluctuations. Keeping this in mind, we analyze only travel-time differences, which are sensitive to flows. In order to estimate these travel-time differences, we perform a calculation of a ray propagating through a model of solar convection, taken from the Anelastic Spherical Harmonic (ASH) code (Miesch *et al.* 2000). Such a calculation also shows us the correlation between the travel-time maps and the convective velocities that the ray samples.

2. Ray calculations

To compute travel-time differences, $\delta\tau$, we use a standard method (e.g. Giles 1998) that applies the following equation:

$$\delta\tau = 2\left[\int_{r_1}^{r_2}\frac{u_h}{c^2}\left(\frac{\omega^2 r^2}{l(l+1)} - c^2\right)^{-\frac{1}{2}}dr + \int_{r_1}^{r_2}\frac{u_r}{c^2}dr\right], \quad (2.1)$$

where r is the radius, u_h is the horizontal flow velocity component in the direction of the propagating ray, u_r is the radial velocity component along the ray path, ω the circular frequency of the acoustic wave, l the spherical harmonic order, c the sound speed, r_1 the lower turning point and r_2 is the upper turning point. For calculations presented here, we approximate $r_2/R_\odot = 1$. The first and second terms on the right-hand-side denote travel time contributions from the horizontal and radial components of the flow, respectively.

2.1. *Deep convection model*

The ASH code computes acoustics-free convection in a spherical shell. By neglecting the rapidly propagating acoustic waves in the convection zone, Miesch et. al. (2000) are able to obtain a significant increase in the computational timestep of the convection simulation. For the ASH profile used in the ray calculation, the computational boundaries were placed at $0.76R_\odot$ and $0.96R_\odot$ and act as no-slip, impenetrable walls. Because of these boundary conditions, the radial velocity vanishes at both ends and it is important to keep this aspect in mind while interpreting the results from the ray calculations. The latitudinal velocity at a radial layer from the ASH simulation is shown on the upper panel of figure 1.

2.2. *Surface convection model*

Acoustic waves spend the longest time in the near-surface layers. These waves are strongly biased by supergranular activity in the sub-photospheric regions. In order to take this effect in account, we model supergranules by cell-like structures with an average horizontal cellular size of 30 Mm and depth of 15 Mm. Each unit acts a 'convective cell', with velocity profiles chosen to satisfy the continuity equation, $\boldsymbol{\nabla}\cdot(\rho_0\mathbf{v}) = 0$ (e.g. Swisdak & Zweibel 1999), where ρ_0 is the solar density, $\mathbf{v}$ the vector velocity and $\boldsymbol{\nabla}\cdot$ the divergence operator. The maximum velocity of a 'supergranular' cell is 200 ms^{-1}. The surface velocity profile is shown in figure 1.

For these calculations, we have taken a snapshot in time from the ASH simulation and apply a constant (in time) surface convection model. One of the reasons we may do this is the decoupling of timescales between the acoustics (5 minutes) and the turnover time of convective cells (several hours to days). Also the long convective cell lifetimes in comparison to the length of the time series of solar data we use to recover the travel-time differences, allows us to invoke the assumption of time constancy.

2.3. *Travel-times*

To determine the travel-time difference associated with a point at a certain depth, we first center an annulus around the surface projection of the desired point. The diameter of the annulus is equal to the horizontal distance traversed by a wave whose inner turning point is r_1, as described in equation (2.1). As shown in figure 2, we then divide the annulus into 4 equal quadrants, two horizontal quadrants ($[2\pi - \pi/4, 2\pi] \cup [0, \pi/4]$ and $(3\pi/4, 5\pi/4]$), and two vertical quadrants ($[\pi/4, 3\pi/4]$ and $(5\pi/4, 2\pi - \pi/4)$). The travel-time differences are divided into two categories, east-west and north-sorth, based on whether the corresponding rays lie in the horizontal or vertical quadrants, respectively. All the
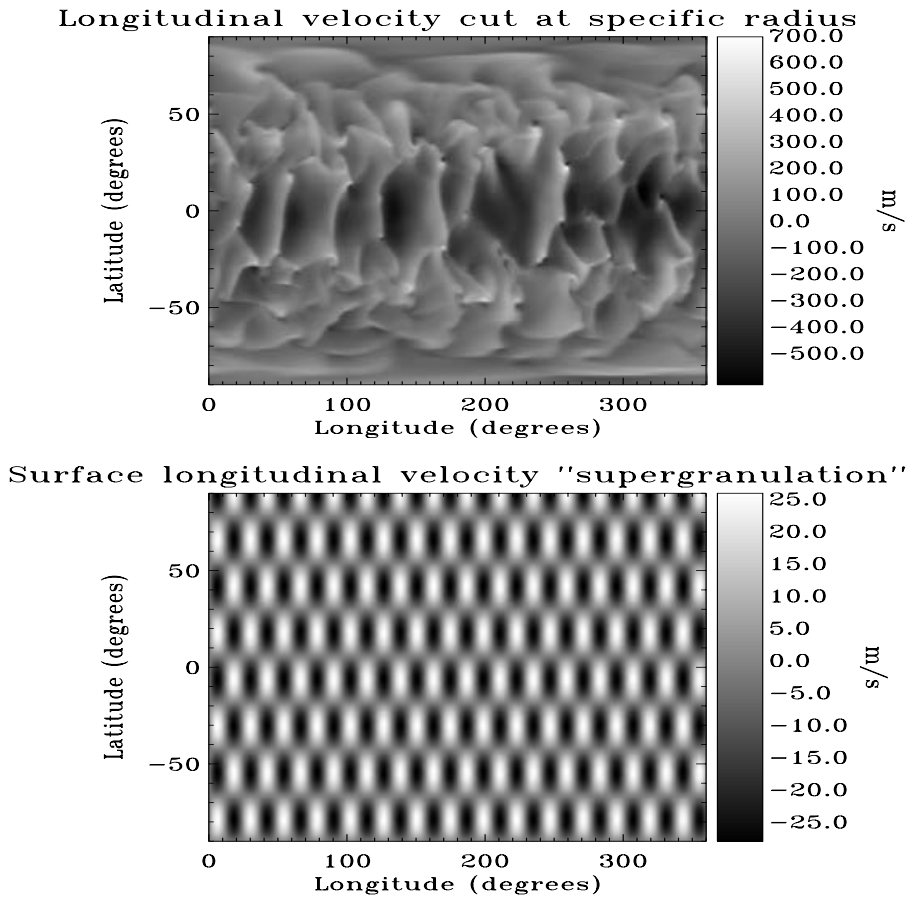
Figure 1. Sections of velocity profiles, dimensions of the scale are in m/s. The upper panel shows the longitudinal velocity taken from the ASH simulation at a single radial cut, corresponding to $r = 0.92 R_\odot$. The lower panel shows the cellular pattern exhibited by the longitudinal velocity at the surface, a crude model for supergranular activity. We use 4 times as many 'supergranules' in our calculations.

east-west travel times are averaged to give a mean east-west travel-time difference. A similar procedure is implemented for the north-south travel-time difference. When dealing with solar data, this procedure helps in reducing the noise.

We use multiple rays with identical frequencies $\omega/2\pi = 3.2$ mHz but differing inner turning points. For a fixed ω, the inner turning point moves closer to the surface as the degree l increases. In figure 3, we show a sample east-west travel-time map for a ray with $l = 128$. On the left panel in figure 4, we show the dependence of the RMS travel times (east-west and north-south) with the inner turning point of the ray.

RMS travel time differences are shown on the left panel in figure 4. The horizontal co-ordinate represents the inner turning point of the ray used to recover these travel times. In general, one may expect that as the coherence of velocity map decreases, i.e. the velocity power is spread over a large range of wave-numbers, travel-time differences and correlations will also decrease. As can be seen in figure 5, the longitudinal velocity power peaks at very low l and decays rapidly with increasing l, while the latitudinal velocity power decays more slowly. The greater clustering of power in the convective
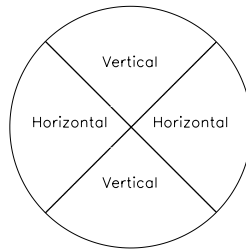
Figure 2. Quadrants used for travel time averaging. East-west rays are defined as those which propagate to from one horizontal quadrant to the other. Similarly, rays that span the vertical quadrants are north-south propagating. After computing the travel times for rays propagating in various directions, they are then averaged and classified according to the quadrant in which they propagate.
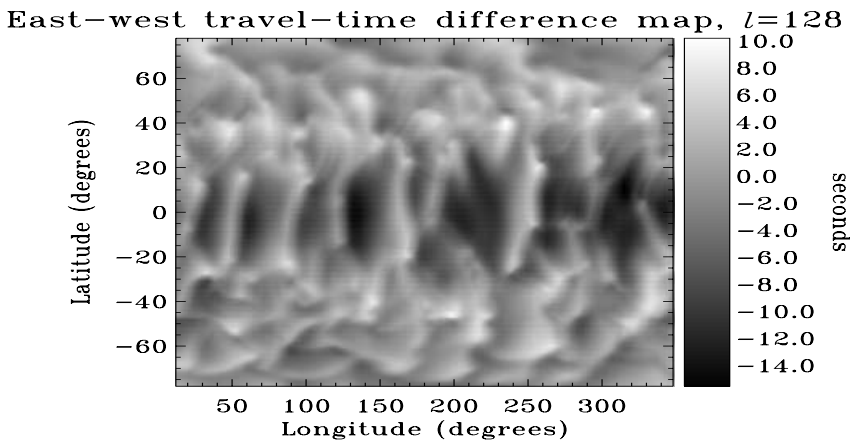

Figure 3. East-west travel-time difference map for a ray with $\omega/2\pi = 3.2$ mHz and $l = 128$ (inner turning point $r_1 = 0.92 R_\odot$). The correlation of the travel-time map with the longitudinal velocity map (see figure 1) at the inner turning point radius is around 0.95, indicating that convective signals are strongly imprinted onto the travel-time differences.

longitudinal velocity than in latitudinal velocities may be the cause of relatively weaker scattering of waves propagating in the longitudinal direction, possibly leading to the differences in east-west and north-south travel times. Furthermore, it may be seen from figure 6 that the longitudinal velocity is consistently larger than latitudinal velocity over the simulation domain, contributing to the larger magnitudes of east-west travel-time differences.

2.4. Correlations

The east-west and north-south travel-time difference maps are then correlated with the longitudinal and latitudinal velocity maps at the lower turning point of the ray in question. Correlations as a function of the inner turning point of the ray are shown on the left panel in figure 4. The correlations decrease as rays with deeper inner turning points are used. It must be noted that the east-west correlations are not always larger than the north-south correlations, as was the case with RMS travel-time differences (see left panel, figure 4). It is interesting to note that the correlation of the shallow rays is very
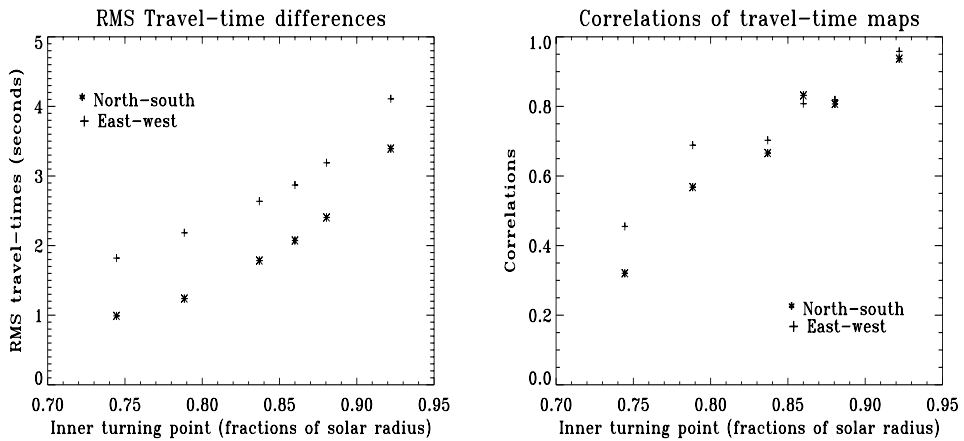
Figure 4. The RMS east-west and north-south travel times on the left panel and correlations with corresponding velocity maps on the right plane, as a function of the inner turning point of the diagnostic ray. It can be seen that the east-west RMS travel times are consistently larger than the north-south travel times for a given ray, sometimes by as much as a factor of 2. The correlations do not follow such a clear pattern though.
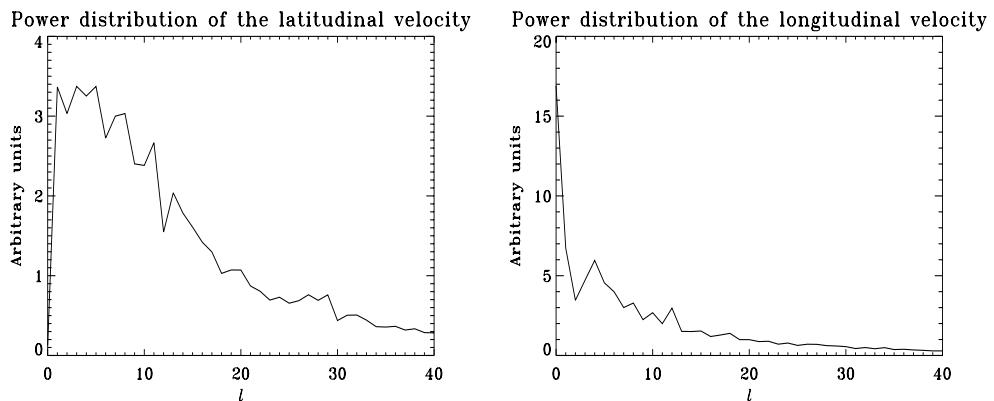

Figure 5. Average power of convective velocities from the ASH simulation (in arbitrary units) for each degree, l at $r = 0.92R_\odot$. While the power increases from the bottom of the domain to the top, the distribution profile is almost constant with radius. The variation of power with wavenumber indicates the extent of the scattering caused by the convection on the propagating rays. The longitudinal velocity power is strongly focused around $l = 1$, indicating that the travel times will preserve the velocity structure of the convection.

high, perhaps indicating that the convective signals are so well preserved in the travel times that inversions are not needed to recover convective structures at this depth.

3. Conclusions

Observing interior convection in the Sun is a very exciting prospect. If we are indeed able to observe these convective cells, even if they are relatively close to the surface, we will be able to understand if current models accurately predict the characteristic sizes of these cells and the associated convective velocities. If we are to believe that the ASH
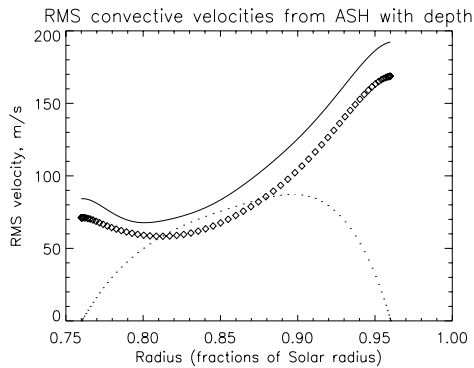
Figure 6. RMS convective radial, latitudinal and longitudinal velocities from the ASH simulation, as a function of depth. The solid line shows the longitudinal RMS velocity, the dots show radial velocity and the symbols depict the latitudinal RMS velocity.

simulations are representative of the solar convection zone, then from the results we obtain, convective signals are strongly imprinted onto the travel-time difference maps. The correlations we obtain in the near-surface regions are so high (∼0.95) that inversions are not necessary to recover the structure of convection at this depth. In terms of real data, we will extract travel times using the deep-focusing technique described in Duvall (2003).

Acknowledgements

References

Beck, J. G., Duvall, T. L., Jr., & Scherrer, P. H. 1998, *ApJ*, 394, 653
Duvall, T. L., Jr., Jefferies, S. M., Harvey, J. W., & Pomerantz, M. A. 1993, *Nature*, 362, 430
Duvall, T. L., Jr. 2003, in: H. Sawaya-Lacoste (eds.), *Local and global helioseismology: the present and future*, Proc. SOHO 12 /GONG+ 2002 (Netherlands: ESA), p. 259
Giles, P. M. 1998, Ph.D. thesis, Stanford University
Miesch, M. S., Elliott, J. R., Toomre, J., Clune, T. L., Glatzmaier, G. A., & Gilman, P. A. 2000, *ApJ*, 532, 593
Swisdak, M. & Zeibel, E. 1999, *ApJ*, 512, 442
van Ballegooijen, A. A. 1986, *ApJ*, 304, 828
Zhao, J. & Kosovichev, A. G. 2004, in: D. Danesy (eds.), *Helio- and Asteroseismology: Towards a Golden Future*, Proc. SOHO 14/GONG 2004 (New Haven :ESA), p. 672

Discussion

ROXBURGH: What is the time scale associated with the convective cells from the ASH simulations? Is it acceptable to use just one snapshot in time?

HANASOGE: It is a reasonable starting point for this calculation. The turnover times of some deep convection cells (close to the bottom of the convection zone) in the ASH simulations is of the order of a month. A simple way to estimate the timescale associated with convective cells is to divide twice the depth of the convective cell by the RMS velocity (longitudinal or latitudinal) at that depth.